A Variable Damping Module for Variable Impedance Actuation

Manuel Catalano[†‡], Giorgio Grioli[†], Manolo Garabini[†],
Felipe Weilemann Belo[†], Andrea di Basco[†], Nikos Tsagarakis[‡] and Antonio Bicchi[†‡]

***Abstract*— Recent robotic research recognized the advantages that Variable Impedance Actuators would yield to a new generation of robots, rendering them adapt to many different tasks of everyday life.**

In this work we present the development of a Variable Damping mechanism, designed to integrate within a modular Variable Stiffness Actuator platform to realize a complete Variable Impedance Actuation unit.

After a short discussion on the possible implementation strategies, the different operation principles and realization methods of damping systems are initially introduced, and a detailed description of the mechatronics and functionalities of a novel variable damping unit follow. In particular, the proposed implementation adopts an innovative aperture mechanism, similar to the light shutter of a camera, to engage a rotating chamber of high-viscosity silicon oil.

Finally, some experiments are shown, to validate and characterize the system.

I. INTRODUCTION

One of the goals of robotics is the development of robots capable of interacting with a non-structured and continuously evolving world, populated by both inanimate and animate objects, to the same extent as humans do.

While robots already surpass humans in many tasks, especially very specific and repetitive factory operations, there are still many simple and common operations for which robots still lack behind humans, rendering their adoption for such assignments still a dream.

An example of the current superiority of humans with respect to their robotic counterparts is their proficiency in sport activities. One of the main factors that keep robots from successfully playing soccer with humans [1][2], for example, is that common robotic actuation systems are limited with respect to muscles. Such deficiencies become more and more evident if aspects like adaptability, energy efficiency and robustness (just to name a few) are taken into account.

As a consequence a substantial amount of research within robotics is recently oriented towards the development of actuation systems that are able to overcome this disparity. While early approaches to robotic actuation consisted in designing systems which, hiding their intrinsic dynamics with control, behaved like ideal trajectory generators (*servomotors*), more recent approaches attempt to exploit properties of natural system dynamics to manage the interaction of robots with the environment [3].

To achieve such interaction in a profitable and efficient manner, robotic actuation systems were then designed to incorporate in their mechanical structure dynamic behaviors that were previously discarded, e.g., the adoption of elastic [4] and dampers [5] proved to highly improve the performance of robotic systems.

Fig. 1. Picture of the via actuator realized coupling a VSA-Cube and the Variable Damping add-on.

These ingenious solutions have the effect of adjusting the output mechanical impedance characteristic of the actuation unit. In early systems the stiffness could only preprogrammed before the task [6] while recently many units [7] have been developed which allow the real time regulation of the stiffness during the execution of the task. This second type of mechanisms is termed Variable Stiffness Actuation (VSA). Other recent devices explore the possibility of varying the damping of the mechanical transmission with applications in haptic interfaces [8] and in human-robot interaction [9]. The need to adapt the damping coefficient between and within different tasks, has different motivations, the possibility to adapt to different loads optimizing the system bandwidth is just the foremost. While system damping can be obtained with suitable control approaches, as in [10], there are reasons which support a physical implementation of the damping principle, for example the benefits of intrinsic system passivity as well as energetic considerations on the power consumption of the link motor. Variable Damping systems along with VSAs illustrate the growing interest of the scientific community in Variable Impedance Actuators (VIA).

This work represents an evolution of this refinement process, that culminates in the first VIA (Fig. 1) capable of adapting both its output stiffness and damping. In particular, the VIA is realized by the application of an independent Variable Damping add-on module to an already existing VSA device, the VSA-CubeBot presented in [11].

The paper is organized as follows: in section II we report a roundup of possible layouts that can be use to implement a variable impedance actuator.

[†] Interdepart. Research Center "E. Piaggio", University of Pisa, Via Diotisalvi, 2, 56100 Pisa, Italy.

[‡] Department of Advanced Robotics, Istituto Italiano di Tecnologia, via Morego, 30, 16163 Genova

In section III we report some different physical principles that can be used to realize a damper. In section IV we report the design of the chosen mechanism and describe the variable damping mechanical implementation. Finally, in section V we report the experimental results.

II. VIA TAXONOMY

Consider a system described by a motor with an output shaft within a containment frame, an elastic connection between the motor and the shaft, and a source of damping action. The three possible configurations of such system are shown in Fig. 2. In this section we present a detailed analysis of these connection topologies and highlight benefits and drawbacks of each solution.

Fig. 2(a) shows a stiffness and a damper in parallel between the reference and the link, Fig. 2(b) presents a stiffness between the reference and the link, and a damper between the link and the external frame. This topology is featured, for example, in models of human limb impedance, as in [12]. Fig. 2(c) present a serial connection of a spring and a damper between the reference and the link. This schema is similar to those adopted in [8] and [5] and presents the advantage of minimizing the amount of motor inertia reflected to the link. Nevertheless, it has the major disadvantage of requiring continuous rotation of the motor to apply a constant torque to the output.

Some other differences arise between the three schemes, for instance, to achieve the behavior of a pure VSA, the damping factor should be null for layouts (a) and (b), while it should tend to infinity for layout (c).

Fig. 3 and 4 show a possible implementation of schemes (a) and (b) of Fig. 2 integrated within the two most common VSA layout, namely Agonist-Antagonistic (A-A) and Explicit Stiffness Variator (ESV). A disadvantage of systems of Fig. 3 is that the variable damping unit must be integrated into the actuator design, moreover the damping action disturbs the stiffness variation, in fact, it is necessary to overcome the damper resistance. One drawback of system Fig. 4 is that, during link motion, the damper resistance must be surpassed. This can be overcame by realizing a variable damping mechanism that can be completely turned off. On the other side, systems of Fig. 4 have the advantage of allowing the designer to realize the variable damping unit as an *add on* which can be attached externally to another actuation unit, as a VSA. For these reasons the layout adopted in this work is 4 (a), which is also the most suitable to be adopted in a modular low cost robotic development platform like the *VSA-CubeBot*.

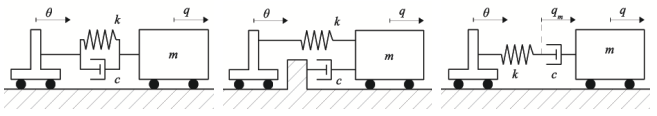

Fig. 2. The three possible layouts to add a damping action to a system coupling a motor with a load through an elastic connection: Pure parallel (a), External parallel (b) and Serial.

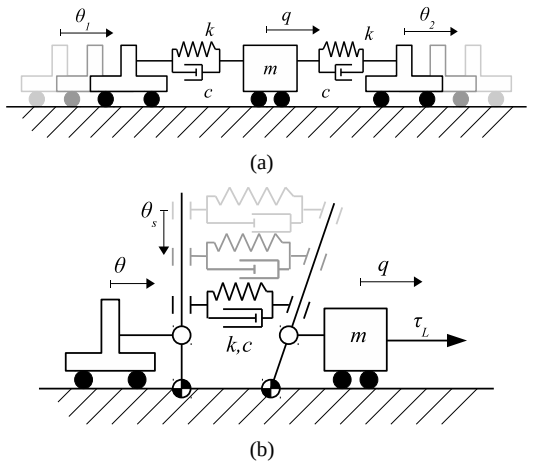

Fig. 3. Implementation of a pure parallel layout to introduce damping in two VSAs: Agonist-Antagonist (a) and Explicit Stiffness Variator (b). The damping element in parallel with the springs can slow-down the stiffness adjustment time by opposing to the springs deformation by the motors.

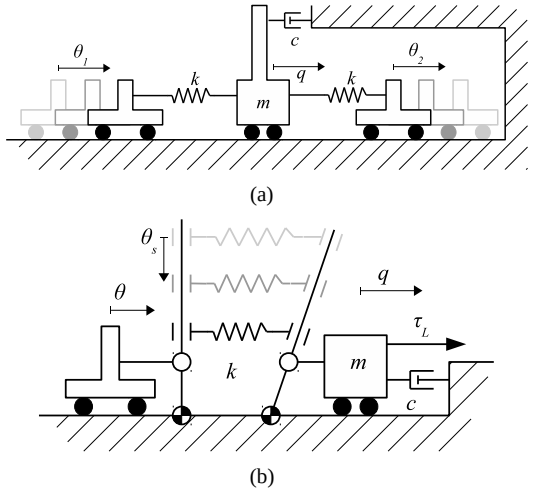

Fig. 4. Implementation of an external parallel layout to introduce damping in two VSAs: Agonist-Antagonist (a) and Explicit Stiffness Variator (b). The schemes show that it is possible to keep the actuation unit unchanged by placing the damping unit between the output link and the frame.

III. OPERATING PRINCIPLES

Dampers have been thoroughly studied over the past centuries and can be realized using different operating principles. Here, we briefly discuss the fundamental ones.

The aim of this study is that of choosing the principle that fits the following system requirements best: to render damping force the closest possible to being proportional to the velocity in order to simplify and reduce control effort; to have compact size; to be easy to assembly; and, to integrate with the VSA-*CubeBot* unit keeping overall cost low.

A. Friction damper

A Friction Damper (FD) is, essentially, composed of an actuator that applies a normal force, F_n, on the output shaft. Frictional damping force F_d is produced as a consequence of relative motion. The simplest model describing the behavior of the FD is

$$F_d = -fF_n sign(\dot{q}_r), \tag{1}$$

where f represents the friction coefficient and $\dot{q}_r$ the relative speed between the actuator and the output shaft. A more complex and realistic mathematical model can be found in [13]. This principle has been used in the design of the actuators presented in [9] and [14]. Drawbacks of FD, pointed out in [13], are the noticeable phenomena of hysteresis and the presence of a static friction band [15] that can cause irregular behavior.

B. Electrorheological and Magnetorheological Dampers

Electrorheological (ER) and magnetorheological (MR) dampers are based on liquids whose physical behaviors depends on the application of electric or magnetic fields respectively [15]. These fluids follow the Bingham models: after a yielding point, they behave as viscous liquids. The property that can be changed is the yield stress itself.

Based on the Bingham viscoplastic model, the behavior of ER and MR fluids can be described by

$$F_d = -sign(\dot{q}_r)(g(\mu,|\dot{q}_r|)+Cu)\,, \tag{2}$$

where $g(\mu,|\dot{q}_r|)$ represents the viscous component of the damping force, μ the viscosity of the fluid, u the electric field or the current for ER and MR respectively and C denotes a coefficient that depends on the physical properties of the fluid and on the geometry of the damper. The MR operating principle is often used to realize VDAs in robotics [5] and also in vehicles [16]. A more accurate model and a comparison between MR and FD can be found in [13], where it is pointed out that MR dampers, like the FDs, present high hysteresis.

C. Eddy Current Dampers

Eddy Current Dampers (ECDs) are magnetic devices composed of a conductive material moving through a magnetic field. Eddy currents are induced and create a damping force that is proportional to the relative velocity $\dot{q}_r$ between the material and the magnetic field

$$F_d = -D(r,d,h,B,\sigma)\dot{q}_r\,. \tag{3}$$

The coefficient D depend, ultimately, on the geometry of the conductor, represented by r, and of the magnet, denoted by d, their gap, h, the magnetic flux, B and the specific conductivity of the conductor σ.

These devices can be realized with both permanent magnets or electromagnets. In both cases there is the possibility to design a device whose damping can be adjusted ([17], [18]). In one case, the damping coefficient can be controlled by varying the intensity of the magnetic field, in the other case, by modifying the geometry of the conductor, or the gap between the conductor and the magnets (the effectiveness is shown in [18]). Albeit electromagnetic ECD are not composed of mobile parts, they have the disadvantage of consuming power while maintaining a fixed damping value.

This class of devices, being fluid-free and contact-free, is not affected by typical troubles due to oils (e.g., the need of seals against leakage), and by frictional wear. Still, they present the disadvantage of requiring a gearbox because of their low damping torque.

D. Fluid dynamics damper

Two main possibilities exist when using fluids to damp: the quadratic damping and the linear damping. The Reynolds number can be used as indicator of the main phenomenon by which the damper works. These two possibilities are described as follows:

- when the fluid is characterized by turbulent flow (high Reynolds number) it produces a damping force proportional to the square of the relative speed

  $$F_d = -sign(\dot{q}_r)C_v{\dot{q}_r}^2\ , \tag{4}$$

  from where the term quadratic damping comes from. A practical example of quadratic damping is a damper with an orifice allowing fluid flow, as largely used in automotive industry. Such device generates, at a given frequency, high damping for high amplitudes, but lower damping for lower amplitudes, and thus, has the drawback of presenting long lasting residual oscillations ([15]).
- *linear damping* is the phenomenon present when a fluid is characterized by laminar flow (low Reynolds number) and produces a damping force proportional to the speed gradient in the fluid.

  $$F_d = -d(\mu,A,h)\dot{q}_r\ . \tag{5}$$

Here, the damping coefficient d mainly depends on three parameters: A the area of the surface in contact with the fluid; h the height of the fluid chamber; and μ, the viscosity of the fluid.

IV. Variable Damper Design

A. Requirements

We chose to implement a linear fluid damper because it produces a damping force proportional to the relative speed, unlike FD, ER, MR and the quadratic fluid damper. This characteristic is important because it allows one to not continuously adjust the device to have a constant damping in a task with a speed variation.

This particularity is also present into the ECDs, yet the formers have been discarded because they would need a gearbox to achieve the required amount of damping values within the desired small space.

In order to have an acceptable number of steps in adjusting the damping, we chose to variate A because variating h would

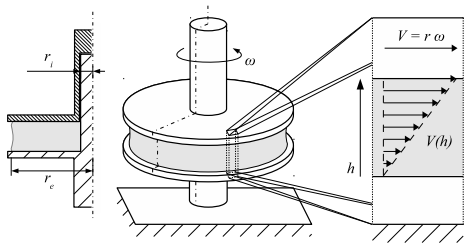

Fig. 5. Scheme of the variable damper. The meatus has an annular shape, r_i and r_e represent the internal and external radius respectively and h is the height. The relative angular speed of the upper and lower surface is denoted by ω while V represents the linear speed shear of fluid film between two flat discs.

require a very fine resolution.

The minimum and maximum damping values are chosen to realize a shoulder joint suitable for a 5-dof arm composed of *VSA-Cube* modules as those presented in Fig. 7 (*b*). We chose the maximum value of the damping range such to stop the free oscillation of the arm starting from a horizontal fully-extended configuration and set to the highest stiffness.

A simplified dynamic model of the arm is a rotating arm of length l, a mass m and inertia I. The system is described by equation

$$I\ddot{q} + d\dot{q} + kq = -Asign(\dot{q}) - mglcos(q)\,, \tag{6}$$

where m represents the total mass of the arm, l is the total length of the arm; k, d and A represent stiffness, damping and Coulomb friction of the shoulder joint; g denotes the gravity acceleration and q the angular position of the shoulder joint.

Simulations, performed with the model of eq. 6 all over the stiffness range, show that, given the values of the parameters ($m = 1.45kg$, $l = 0.4m$ and $k = 3-14Nm/rad$, $A = 0.1Nm$), oscillations characterized by a period of $0.5s$, overshoot 90% and settling time $6s$ arise. The damping value needed to critically damp such oscillation is our target maximum damping, $d_{max} = 0.6Nms/rad$.

On the other hand, the ideal minimum value for the damping coefficient would be, given the considerations in Sec. II, that of zero damping.

Practical reasons hint a rotational geometry for the damper, following the working principle of Fig. 5. This kind of system works as a parallel disc viscometer [19] that generates a damping torque described by the following equation (refer to Fig. 5 for definitions)

$$T_d = \frac{\mu\pi\left(r_e^4 - r_i^4\right)}{2h}\omega\,, \tag{7}$$

and yielding the following expression of the damping coefficient

$$d = \mu\pi\frac{r_e^4 - r_i^4}{2h}. \tag{8}$$

By varying the gap area and/or height, it is possible to change the damping factor. The best performance, in terms of damping range and damping stability, is obtained by employing a Newtonian fluid because, in such fluids, viscosity is time and velocity independent. However, the viscosity range of these fluids is not sufficient to respect the dimensional design constraints, so the usage of high viscosity fluids, such us silicone oils, is necessary. These materials present a non-Newtonian behavior; in particular, silicone oils present a shear thinning behavior (apparent viscosity decreases with velocity). However, as it is also shown in experimental tests of Fig. 12, these fluids present a transient high viscosity phase when velocity is increasing. This particular property can be used in system, like ours, where the rotation of the output shaft is limited and movements are pseudo-periodic.

Design constraints, manufacturing limits and non-newtonian behavior of the fluid impose the following constraints on the dimensions of the fluid chamber: $r_e < r_{e,max} = 25mm$, $r_i > r_{i,min} = 14mm$, $h > h_{min} = 0.5mm$.

Given design constraints it is possible to evaluate the minimum value of fluid viscosity, μ_{min}, such that d_{max} can be achieved

$$\mu_{min} = \frac{d_{max}h_{min}}{\pi * \left(r_{e,max}^4 - r_{i,min}^4\right)} \approx 400\,[Pas]\,. \tag{9}$$

A silicone oil with a viscosity of $500\,[Pas]$ was used to implement the device.

B. Mechanical Design

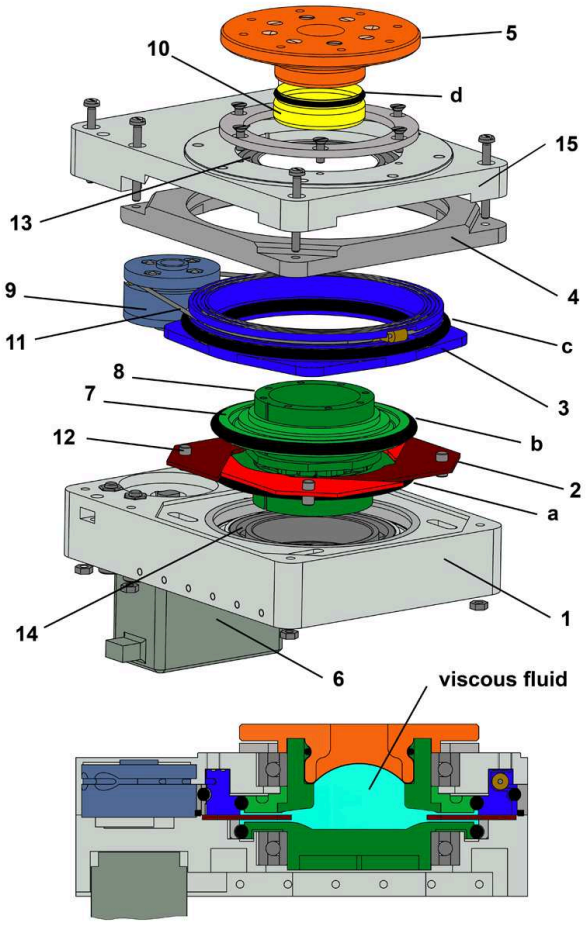

Fig. 6. Exploded 3D view and section of the variable damping system with basic components highlighted. The viscous fluid is represented in light blue. The laminar fluid shear is generated between petals 2 and rotors 8, 7.

As stated in previous sections, the basic goal behind the system development is to obtain a modular damping unit that can be integrated with the VSA-*CubeBot* system (e.g. in the shoulder), and change the damping value by changing the fluid chamber area. To deal with these two main features the adopted mechanical solution is inspired by the aperture mechanism, as those used in cameras.

Fig. 6 shows an exploded view of the variable damping system. The module has two main frames (1 and 15), which implement the connection with the VSA-*Cube* module, as in Fig. 7 (*a*), and the integration with the *Qboid* platform as in Fig. 7 (*b*). In particular, the output shaft of the VSA-*Cube* module is rigidly attached to the rotor of the damping system (8), which is mounted on frames 1 and 15 by two ball bearings. A large flat surface on component 8 creates

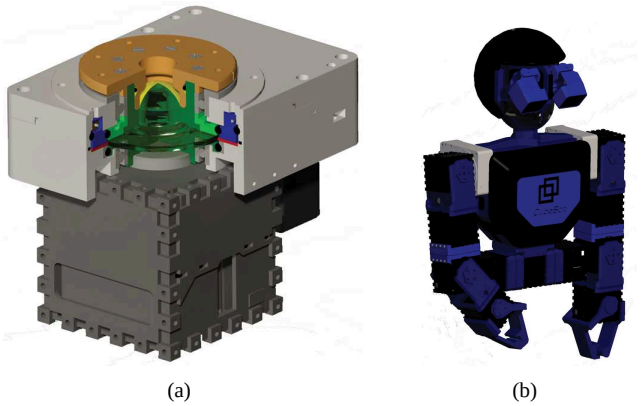

(a) (b)

Fig. 7. On the right side is depicted a 3D section of the variable impedance add-on system mounted on the VSA-*Cube* module (a). On the left is showed the VSA-*CubeBot* platform implementing two add-on in the shoulders (b).

a shear chamber filled with fluid when the four aperture petals (2) are engaged. Part 7, fixed on the rotor axis, forms another chamber on top of the petals. Along the maximum diameter of 8 and 7, two O-rings *a* and *b* prevent the viscous fluids from leaking from the chambers. The aperture system is actuated by component 3, which is constrained to rotate around its axis, that coincides with rotor axis 8. Part 3 is moved by a wire transmission system (11) actuated by a motor (6) with a pulley (9), fixed on it. Petals 2 are linked to 3 by four pins (12), one for each petal. These pins can translate along prismatic guides grooved on the surface of 1. Part 4 closes the aperture system region (through the O-ring *c*) and realize a hermetic volume. Hence, the viscous fluid is contained in the chamber formed by the inside of rotor 8, and the regions delimited by 1, 8, 4 and 7. The volume inside rotor 8 is closed by a rubber elastic membrane (10), fixed on 8 by the output shaft of the damping system 5, and forms a recovery chamber.

Fig. 8 shows three different operating conditions of the damping mechanism. When the system is set to low damping configuration the aperture is completely open and both the chamber and the recovery chamber are filled with fluid. When the aperture system is actuated, petals move inside the rotating chamber pushing the moved fluid inside the recovery chamber in 8. When petals return to an open configuration, the fluid returns from the recovery chamber in 8 to the rotary chamber.

The logical scheme illustrating the working principle of the closure mechanism is shown in Fig. 9. The relation between the angular displacement of the motor and the damping coefficient is

$$d = \mu\pi \frac{r_e^4 - \left(\frac{a}{\cos(\theta_m/\rho)}\right)^4}{2h} \tag{10}$$

where θ_m represents the angular displacement of the motor, $\rho = 3$ represents the reduction ratio between the motor pulley and the element 3 and a is defined as in Fig. 9. The angle from the maximum to the minimum damping configuration that the motor must provide is about 30°.

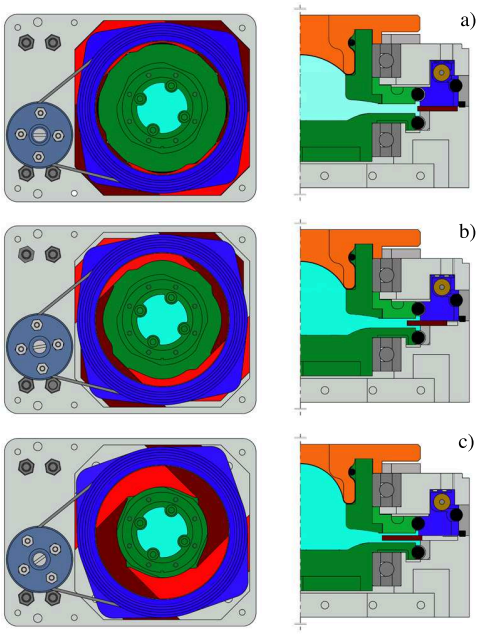

Fig. 8. Three different position of the aperture mechanism: *a*) 0%, *b*) 20% and *c*) 100%. During the closure movement petals push the fluid in to the recovery chamber under the rubber membrane. When the system return to 0% closure position the fluid goes out from the recovery chamber and refills recovery chamber.

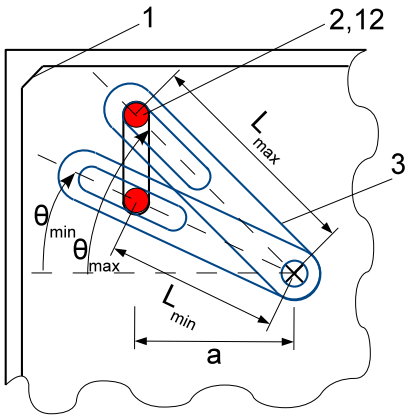

Fig. 9. Scheme of the aperture mechanism. The blue element represents the element 3, the red element represents one of the petals 12 with the pin 2, the black element represents the frame 1. The output-shaft center to pin center distance at the minimum damping configuration is $L_{max} = 35$ [mm], at the maximum damping configuration is $L_{min} = 32$ [mm]. The distance between the output-shaft center and the prismatic guide on the frame 1 is $a = 24.7$ [mm]. The angles $\theta_{min} \approx 35°$ and $\theta_{max} \approx 45°$ are relatives to the maximum and minimum damping configuration, respectively; hence the maximum angular displacement of part 3 is about 10°.

V. Experimental Tests

A. Variable Damping Experimental Setup

To characterize and validate the VD device, a simple experimental set-up was realized in which the rotor 8 was actuated and both the rotation speed of the rotor and the holding torque on the frame 1 were recorded, for different rotation speeds and closure levels of the aperture system.

The rotor was moved by a SUN 454-0899 12V DC motor. The rotor speed was computed by direct differentiation of the

rotor position which is monitored by an HEDS 5540 optical encoder, and the holding torque was acquired with a strain gauge connected to a Mecmesin 460-1427 Force and Torque test device. Data was acquired with a Phidgets ic board and analyzed with Matlab-Simulink software.

Two kind of experiments were done: in the first experiment (experiment 1), in order to characterize the range of damping with respect to speed, the rotor is controlled using a sine-wave speed reference, characterized by a period of $2Hz$ and an amplitude of $2.6rad/s$ and a total duration of 10 seconds. In the second experiment (experiment 2), in order to evaluate the transitory response of the damper due to the time dependent behavior of the damping fluid, the rotor is controlled to a fixed speed reference of $2.6rad/s$ for a duration of 30 seconds.

B. Variable Damping Experimental Results

Results of experiments 1 and 2 are reported in Fig.s 10 and 11. The numerical derivation of data from experiment 1 (Fig. 10) is the damping coefficient as a function of velocity as shown in Fig. 11. From figures Fig.s 10 and 12, the range of damping corresponding to different operating conditions can be derived: the damping coefficient ranges from a minimum of $0.15Nms/rad$ to a maximum of $0.4Nms/rad$. Noticeably, a certain amount of hysteresis is present. This hysteresis is, nevertheless, comparable to the hysteresis found in most commercial viscous dampers, which is in the order of 50%. This hysteresis is partially due to the transitory behavior of the damping fluid which can be characterized from Fig. 11. A decay of about 50% within a time of 6-7 s can be measured.

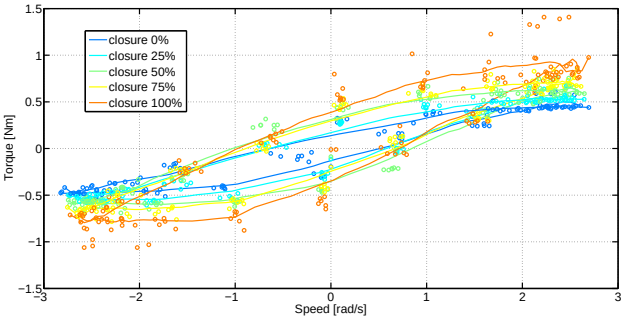

Fig. 10. Experimental mechanical characteristic of the variable damper. The 5 different colors are obtained for 5 levels of petal closures. The dots are obtained by collecting data during the accelerating and decelerating phases of a periodic sine-wave motion with a period of $2s$ and a maximum speed of about $2.6rad/s$, respectively. The lines are obtained mediating and filtering the dots data.

C. Variable Impedance Experimental Setup

In this final experiment set, the Variable Damping module presented in the previous part of the work is mounted on top of the VSA-*Cube*, as shown in Fig. 1 and 7 (a), realizing a complete VIA, with the possibility to adjust both its output stiffness and damping. The system was used to move a load with similar inertia to that of the arm of the robot shown in Fig. 7 (b). The equivalent inertia of $0.077Kgm^2$ is moved to track an angular step of $80deg$ with different stiffness and damping values.

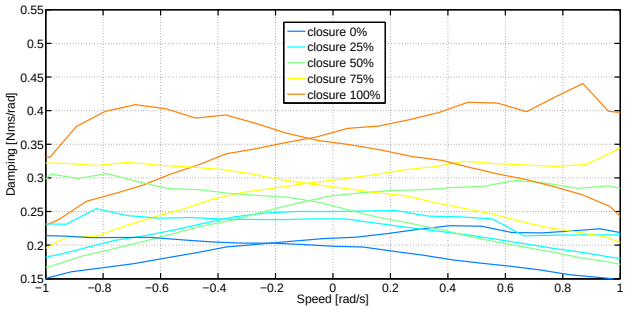

Fig. 11. Experimental damping for the variable damper, as extracted from data of figure 10. The two lines of each color are relative to the ascending and descending traits of data in figure 10. Due to noise in the acquired data, numerical derivation of the mechanical characteristic has been performed just on the central part of the acquired speed range.

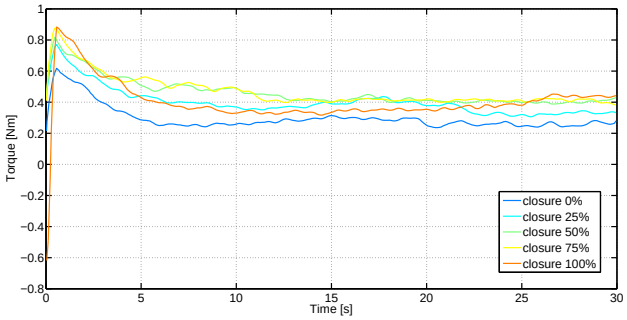

Fig. 12. Experimental torque decay on the variable damping when continuously opposing to a constant speed of approximately $2.6rad/s$. The torque decay is due to natural transitory phenomena inside the damping fluid.

D. Variable Impedance Experimental Results

Fig. 13 shows experimental results of the system with constant maximum damping and different values of stiffness (Fig. 13 (a)), constant minimum damping and different values of stiffness (Fig. 13 (b)). Fig. 14 shows experimental results of the system with constant maximum stiffness and different values of damping (Fig. 14 (a)) and constant minimum stiffness and differnt values of damping (Fig. 14 (b)). From the figures it is noticeable the influence of different values of damping and stiffness, especially in terms of the overshoot, which can be contained both with decreasing values of stiffness (Fig. 13) or with increasing values of damping (Fig. 14).

VI. Conclusion

This paper presented a variable vamping device that can be integrated with an existing variable vtiffness actuators, the *VSA-Cube* module. By combining these two devices a physical Variable Impedance Actuator is obtained. The design and the mechanical realization, as well as the functional details were illustrated, along with the main performance parameters. Experimental results validating the effectiveness of the system were reported.

VII. Acknowledgments

The authors gratefully acknowledge the contribution of Fabio Bonomo, Michele Mancini and Fabio Vivaldi. Work

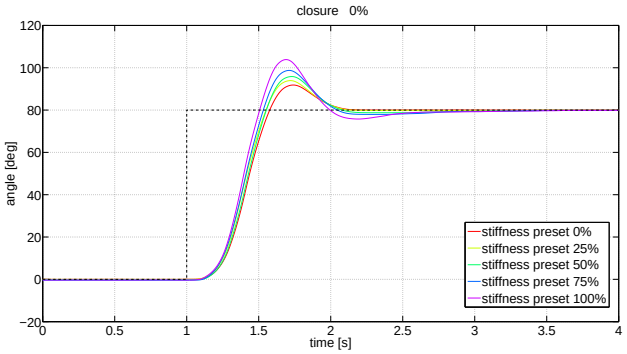

(a)

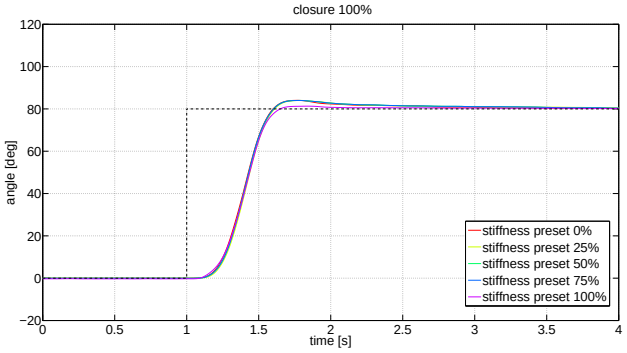

(b)

Fig. 13. Experimental step response results at: (a) minimum damping and different stiffness preset values, (b) maximum damping and different stiffness preset values.

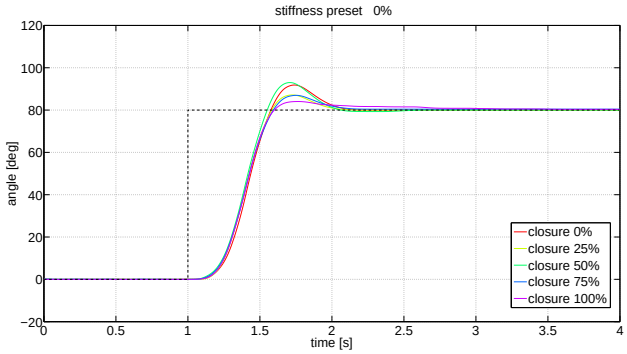

(a)

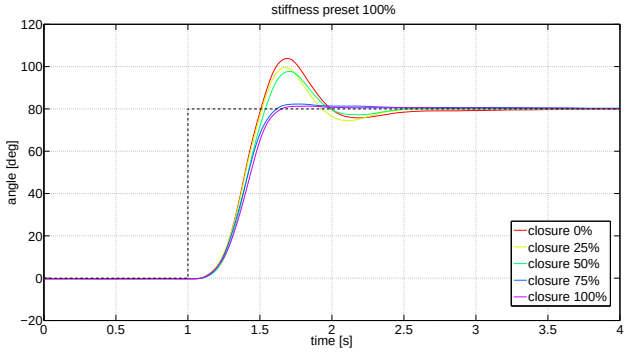

(b)

Fig. 14. Experimental step response results at: (a) minimum stiffness preset and different damping values, (b) maximum stiffness preset and different damping values.

supported by the European Community, under grants FP7 ICT-231554, "VIACTORS", FP7 ICT-287513 "SAPHARI" and FP7 ICT-248587, "THE Hand Embodied".

REFERENCES

[1] H. Kitano and M. Asada, "Robocup humanoid challenge: that's one small step for a robot, one giant leap for mankind," in *Intelligent Robots and Systems, 1998. Proceedings., 1998 IEEE/RSJ International Conference on*, 1998, pp. 419–424.

[2] S. Haddadin, T. Laue, U. Frese, and G. Hirzinger, "Foul 2050: Thoughts on physical interaction in human-robot soccer," in *2007 IEEE/RSJ International Conference on Intelligent Robots and Systems*. IEEE, 2007, pp. 3243–3250.

[3] Hogan, "Impedance control: An approach to manipulation," in *American Control Conference, 1984*, 1984, pp. 304–313.

[4] D. Robinson, J. Pratt, D. Paluska, and G. Pratt, "Series elastic actuator development for a biomimetic walking robot," in *Advanced Intelligent Mechatronics, 1999. Proceedings. 1999 IEEE/ASME International Conference on*, 1999, pp. 561–568.

[5] C.-M. Chew, G.-S. Hong, and W. Zhou, "Series damper actuator: A novel force control actuator," in *2004 4th IEEE/RAS International Conference on Humanoid Robots*. IEEE, 2004, pp. 533–546.

[6] T. Morita and S. Sugano, "Design and development of a new robot joint using a mechanical impedance adjuster," in *Robotics and Automation, 1995. Proceedings., 1995 IEEE International Conference on*, 1995, pp. 2469–2475.

[7] R. Ham, T. Sugar, B. Vanderborght, K. Hollander, and D. Lefeber, "Compliant actuator designs," *IEEE Robotics & Automation Magazine*, vol. 16, no. 3, pp. 81–94.

[8] A. H. C. Gosline and V. Hayward, "Eddy current brakes for haptic interfaces: Design, identification, and control," *IEEE/ASME Transactions on Mechatronics*, vol. 13, no. 6, pp. 669–677, 2008.

[9] M. Laffranchi, N. Tsagarakis, and D. Caldwell, "A variable physical damping actuator (vpda) for compliant robotic joints," in *Robotics and Automation (ICRA), 2010 IEEE International Conference on*, 2010, pp. 1668–1674.

[10] F. Petit and A. Albu-Schaffer, "State feedback damping control for a multi dof variable stiffness robot arm," in *Robotics and Automation (ICRA), 2011 IEEE International Conference on*. IEEE, 2011, pp. 5561–5567.

[11] M. G. Catalano and G. Grioli, "Vsa-cubebot: A modular variable stiffness platform for multiple degrees of freedom robots," in *Robotics and Automation (ICRA), 2011 IEEE International Conference on*, 2011, pp. 5090–5095.

[12] G. Venture, K. Yamane, Y. Nakamura, and M. Hirashima, "Estimating viscoelastic properties of human limb joints based on motion capture and robotic identification technologies," in *Intelligent Robots and Systems, 2007. IROS 2007. IEEE/RSJ International Conference on*. IEEE, 2007, pp. 624–629.

[13] E. Guglielmino, C. Stammers, and K. Edge, "Damp-by-wire: magnetorheological vs friction dampers'," *16th IFAC World*, 2005.

[14] M. Laffranchi and N. Tsagarakis, "A compact compliant actuator (compact^{TM}) with variable physical damping," *robolab.cse.unsw.edu.au*.

[15] J. C. Dixon, *The Shock Absorber Handbook*, ser. Senior Lecture in Engineering Mechanics, Wiley, Ed. PEP and Wiley, Aug. 2007.

[16] J. Li, D. Jin, X. Zhang, J. Zhang, and W. Gruver, "An electrorheological fluid damper for robots," in *Robotics and Automation, 1995. Proceedings., 1995 IEEE International Conference on*, 1995, pp. 2631–2636.

[17] B. Ebrahimi, M. B. Khamesee, and F. Golnaraghi, "A novel eddy current damper: theory and experiment," *Journal of Physics D: Applied Physics*, vol. 42, no. 7, p. 075001, 2009.

[18] H. A. Sodano, J.-S. Bae, D. Inman, and K. Belvin, "Improved concept and model of eddy current damper," *Transaction of the ASME*, vol. 128, 2006.

[19] G. Leblanc, *Viscosity Measurement*, ser. The Measurement, instrumentation and Sensors Handbook, C. Press, Ed., 1999.